The Effect of Friction on the Forward Dynamics Problem

Pierre E. Dupont
Aerospace and Mechanical Engineering
Boston University
Boston, Massachusetts 02215

Abstract

This article discusses the numerical solution of the forward dynamic equations of an n-degree-of-freedom manipulator with friction. Also discussed are the modeling and experimental identification of friction. It is shown that the inclusion of Coulomb-type friction in the dynamic equations introduces two difficulties in the forward dynamic solution. The differential equations are shown to be discontinuous in the highest-order derivative terms. In addition, the load dependency of this type of friction typically causes the equations to be implicit in the joint accelerations. For the important case of load-dependent transmission friction, the equations can be explicit. Techniques for the forward solution are described through the example of a roller screw transmission. Experimental and simulation results are used to show the importance of load-dependent friction in a particular robot.

1. Introduction

While often neglected because it is difficult to model and poorly understood, friction is present to some degree in all mechanical systems. In robots, it can consume a major portion of the applied torque. For the robot discussed in this article, friction can represent one third of the motor torque.

The effect of friction on robot performance is well known. The static-kinetic friction transition near zero velocity causes stick-slip behavior that limits the fidelity of position and force control. In addition, the load and velocity dependence of friction degrade the tracking ability of simple controllers. As performance criteria are made more stringent and payload-to-arm mass ratios increase, friction becomes increasingly difficult to ignore.

A better understanding of friction phenomena is crucial to understanding and improving robot performance. Incorporating friction models into robot dynamic simulation provides a means to study these issues. For example, simulation models can be a useful tool for robot evaluation as well as for mechanism and controller design. In addition, simulation is becoming increasingly important for planning and verifying remote manipulation tasks.

A significant amount of literature exists on the topic of simulating mechanical systems without friction. An important example is Walker and Orin (1982). The simulation of friction has also received attention. The following paragraphs describe how this work has addressed the issues of friction discontinuity and normal-force dependence.

Discontinuous equations are more difficult to integrate numerically than continuous equations. They can require more complicated algorithms, shorter time steps, and more iterations during each time step. As a result, researchers have proposed continuous approximations to discontinuous friction behavior. If the model is also made state dependent, the problem of normal-force dependence is avoided, too. For example, Luh et al. (1980) represent friction as a continuous viscous damping term.

A more general approach is to replace the discontinuity of the static-kinetic model in Figure 1*A* by a curve of finite slope (Threlfall 1978; Haessig and Friedland 1990). If the slope is large, small step sizes are needed, and the numerical integration remains slow. In addition, the model does not provide a true stiction mode. The system creeps through zero velocity instead of sticking.

Several techniques have been proposed to include stiction while minimizing the effect of the discontinuity on the integration. Karnopp's (1985) model imposes stiction in a small neighborhood of zero velocity. This model allows discontinuity of static to kinetic friction force at the neighborhood boundary. A second approach is based on experimental observations that, near zero velocity, friction is a continuous function of displacement (Threlfall 1978; Haessig and Friedland 1990). If very small displacements are to be accurately simulated, these position-dependent models could be more accurate than a velocity-dependent one.

Several authors have addressed the dependence of friction on normal loads (reaction forces) in the context of digital simulations. Threlfall (1978) proposes a predictor-corrector method that uses the reaction forces from the previous seven time steps to predict the new values. Al-

The International Journal of Robotics Research,
Vol. 12, No. 2, April 1993,

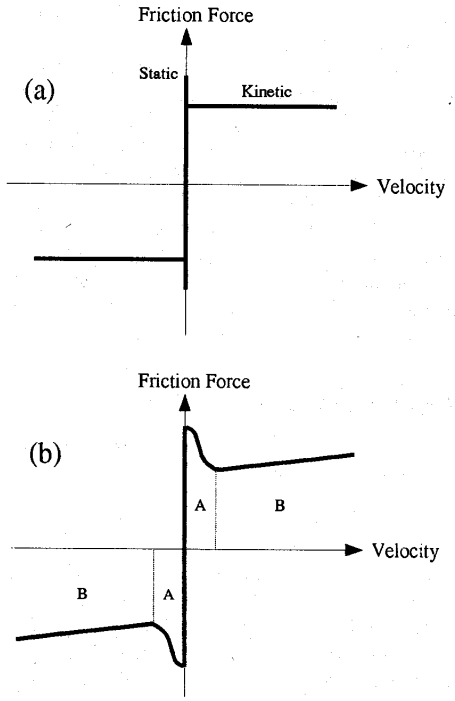

Fig. 1. Friction force versus velocity. A, Static-kinetic model. B, Complex model.

though usually no more than two iterations are needed, friction increases simulation time by a factor of two or three. In a similar fashion, Morgowicz (1988) uses a Newton-Euler algorithm to compute the normal forces for the preceding time step, which are used as a prediction of the current values. He also obtained convergence in at most two iterations.

A hybrid computer scheme is employed in Gogoussis and Donath (1990b) to avoid an iterative solution. These authors have also studied the dependence of normal forces on joint accelerations. Gogoussis and Donath (1987) show that frictional normal force is linearly dependent on joint accelerations. In a second article (Gogoussis and Donath 1988), they show that the friction terms involving normal force will appear as expressions involving absolute values or the square root of sums of squares of joint accelerations.

The remainder of this article is arranged as follows. Section 2 discusses friction modeling. In Section 3, two important points are made. First, the inclusion of discontinuous friction models in the manipulator dynamic equations can cause the joint accelerations to be discontinuous. Second, the inclusion of load-dependent friction models in the manipulator dynamic equations can cause the equations to be implicit in the joint accelerations. Simple examples are used to illuminate these concepts. Switching functions are described as a simple technique for integrating discontinuous ordinary differential equations. Solution existence and uniqueness are discussed as well.

The special case of load-dependent friction and stiction in transmission elements is discussed in Section 4. It is shown that the manipulator dynamic equations can be explicit in the joint accelerations. In the worst case, the accelerations can be computed in a fixed number of iterations. The explicitness of transmission friction is presented in the context of a screw drive. The importance of load-dependent friction is considered through the example of the roller screw transmissions in the Field Materiel Handling Robot (FMR). Section 5 describes the effects of combining transmission friction with other sources of friction at a joint. Section 6 discusses the experimental identification of the FMR's friction parameters and provides a qualitative comparison with robot friction behavior previously reported in the literature. Section 7 presents a summary and conclusions.

2. Friction Modeling[1]

Friction is present in power transmission elements such as gears and screws as well as in bearings, seals, hydraulic components, and electric motors. Friction behavior in each of these is a complex phenomenon. For example, friction in rolling-element bearings is a function of bearing size, type, and design. Additional factors include speed, load type, and magnitude as well as lubricant viscosity and flow (Szeri 1980). While friction can be a function of many variables, in some important cases, it has been shown to be highly repeatable (Armstrong-Hélouvry 1991; Canudas De Wit et al. 1991). Thus friction modeling and parameter identification are not unattainable goals.

Some researchers and manufacturers have developed theoretical or empirical friction models for machine elements and complete systems, as well as typical values of the model parameters. These parameter values provide only rough estimates of the behavior in a particular system. While it may be possible to use them to identify the dominant sources of friction in a system, the actual parameter values should be identified by experiment.

Because of the complexity of friction models in individual components, robotics researchers typically consider an aggregate friction model for each robot joint. This can

1. Portions of this section have been reprinted with permission from *Proc. 1990 IEEE Int. Conf. Robotics and Automation*, Cincinnati, May, 1990, pp. 1370–1376. ©1990 IEEE.

be as simple as the static-kinetic friction model shown in Figure 1*A* or as detailed as that shown in Figure 1*B*.

The limited experimental modeling work in the literature suggests that Figure 1*B* is more appropriate. Friction decreases with increasing velocity in region A of Figure 1*B*. The negative slope makes stable control in this region very difficult. For moderate velocities, friction is reported to increase smoothly with velocity. In this region, labeled B in Figure 1*B*, friction can be thought of as a combination of Coulomb and viscous friction. The shape of this curve is attributed to the transitions between lubrication regimes as velocity is increased (Armstrong-Hélouvry 1991).

It should be noted that Figure 1*B* represents steady sliding behavior. In addition to depending on current velocity, friction depends on the past history of motion. (See, for example, Ruina [1983]; Hess and Soom [1990]; Dupont [1991]). If one is interested in predicting the stability of low-velocity motion in the stick-slip regime, this behavior should be included in the friction model. If the trajectories of interest pass quickly through the negatively sloped region of Figure 1*B*, transient friction behavior can be ignored, since its time scale is short compared with that of the rest of the system.

A second caveat on the models in Figure 1 is that, at velocity reversals, friction may be more appropriately modeled as a continuous function of displacement. This can be interpreted as the straining and eventual rupture of many small bonded contacts between the two sliding or rolling surfaces. The hysteresis models of ball bearings obtained by Dahl (1977) and Walrath (1984) are representative. The transition displacement from static to kinetic friction is on the order of 1 to 10 μm (Armstrong-Hélouvry 1991). It can be an important aspect of the friction model for high-precision tasks such as those of pointing and tracking mechanisms.

By considering the standard Coulomb friction equation, we can gain insight into the computational issues involved in simulating a broad class of friction models. Independent of the area of contact, the Coulomb friction force always opposes relative motion and is proportional to the normal force of contact (Adamson 1982). This force can be expressed as

$$F_C = \mu |F_N| \operatorname{sgn}(v_r), \tag{1}$$

where μ is the coefficient of friction, F_N is the normal force, and v_r is the relative velocity. The signum function is defined as

$$\operatorname{sgn}(x) = \begin{cases} +1, & x > 0 \\ 0, & x = 0 \\ -1, & x < 0 \end{cases} \tag{2}$$

Because of its dependence on the sign of velocity, the friction force is discontinuous at zero velocity. This indicates that the governing differential equations are discontinuous in the highest-order derivative terms.

In addition, the normal forces in robot components depend not only on joint positions and velocities, but also on accelerations. The significance of this normal-force dependence has not been thoroughly studied. Some experiments have shown that friction is independent of normal force (Armstrong-Hélouvry 1991; Canudas De Wit et al. 1991). Our analysis indicates that it is important in certain transmission elements. Its importance in bearing friction is unclear. If present, it will most likely be apparent for heavy payloads or at high velocities and accelerations when dynamic loading is greatest.

3. Robot Dynamics With Friction

The rigid-body dynamic equation including friction for an open-kinematic-chain robot is of the form

$$\tau = D(q)\ddot{q} + h(q, \dot{q}) + f(q, \dot{q}, \ddot{q}). \tag{3}$$

The vectors of joint displacements and actuator torques are q and τ, respectively. Their dimension equals the number of degrees of freedom of the robot. The configuration-dependent inertia matrix is denoted by D. It is both symmetric and positive definite. The vector h consists of centrifugal, Coriolis, and gravity terms. The vector f includes all friction terms and is a function of joint positions, velocities, and accelerations.

The *inverse dynamics problem* is to solve for the joint torques or forces given the joint positions, velocities, and accelerations. Efficient solution of this problem is necessary for model-based control. Regardless of the friction model used, inclusion of the frictional term does not substantially increase the difficulty of the problem if the Newton-Euler recursive equations are employed. In this method, the velocities and accelerations of the links are successively computed from the base outward. Using these quantities, the forces and moments at the joints are computed from the distal link inward. Consequently, the reaction forces and moments are readily available for use in computing the frictional torques.

The *forward dynamics problem* is to solve for the joint positions, velocities, and accelerations given the input torques or forces and the initial conditions. This is the problem to be solved for simulation. At each time step, the known joint torques, positions, and velocities are used to compute the joint accelerations. In the absence of friction, a solution of the type described in Walker and Orin (1982) involves solving a set of linear algebraic equations for the accelerations. Given the special properties of the mass matrix, this can be done efficiently. For example, the Cholesky decomposition method takes advantage of the matrix's symmetry and positive definiteness (Rice

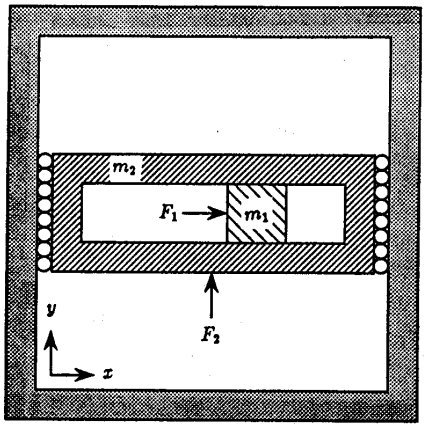

Fig. 2. X-Y positioning system.

1983). Using the values of acceleration and velocity, numerical integration yields the velocity and position at the next time step.

In contrast to the inverse problem, friction can significantly increase the difficulty of solving the forward dynamic problem. Because the resultant forces between the links vary with the positions, velocities, and accelerations of all the joints, the Coulomb-type friction term, $f(q, \dot{q}, \ddot{q})$ in (3), is discontinuous. The left side of (3), $\tau(t)$, can be arbitrarily specified. Clearly, if $\tau(t)$ is chosen as a continuous function, the right side must also be continuous indicating that $\ddot{q}$ can be discontinuous. Furthermore, the form of $f(q, \dot{q}, \ddot{q})$ typically prevents (3) from being solved explicitly for $\ddot{q}$.

3.1. Example 1. Discontinuities in the Forward Solution: X-Y Positioning System

Let us investigate the discontinuity with respect to the highest order derivatives by considering the X-Y Positioning System pictured in Figure 2. While this system employs prismatic joints, the results showing discontinuities in acceleration caused by friction also hold for revolute joints. The equations are more complicated for revolute joints, however, since friction would be velocity- as well as acceleration-dependent.

Referring to Figure 2, mass m_1 moves in the x-direction within the slot in mass m_2, and m_2 moves in the y-direction within the square frame. The forces F_1 and F_2 are applied to the masses as shown. For the sake of simplicity, gravity is not included in this analysis. First consider the frictionless case. Summing forces in the x and y directions, one can obtain the dynamic equation below:

$$\begin{bmatrix} F_1 \\ F_2 \end{bmatrix} = \begin{bmatrix} m_1 & 0 \\ 0 & (m_1 + m_2) \end{bmatrix} \begin{bmatrix} \ddot{x} \\ \ddot{y} \end{bmatrix}. \tag{4}$$

Now let us include a Coulomb-friction force between m_1 and m_2 dependent on the normal force of contact. We can express this force as

$$F_f = \mu |F_N| \operatorname{sgn}(\dot{x}). \tag{5}$$

The discontinuity in this expression is due to the term $\operatorname{sgn}(\dot{x})$. With friction, the dynamic equations become

$$\begin{bmatrix} F_1 \\ F_2 \end{bmatrix} = \begin{bmatrix} m_1 & 0 \\ 0 & (m_1 + m_2) \end{bmatrix} \begin{bmatrix} \ddot{x} \\ \ddot{y} \end{bmatrix} + \begin{bmatrix} \mu m_1 \operatorname{sgn}(\dot{x}) |\ddot{y}| \\ 0 \end{bmatrix}. \tag{6}$$

Notice that the discontinuity does indeed affect the acceleration. In addition to showing a dependence on $\operatorname{sgn}(\dot{x})$, the equation also depends on $\operatorname{sgn}(\ddot{y})$. In this case, however, $\operatorname{sgn}(F_2) = \operatorname{sgn}(\ddot{y})$. For this reason and (as explained in Section 3.2) because the direction of F_N is fixed in a local coordinate frame attached to m_2, (6) is explicit in the accelerations.

As an illustration of the discontinuity and load dependence of Coulomb friction, the behavior of m_1 has been simulated using the parameter values listed below.

$$m_1 = 10 \quad F_1 = 8 \sin(2.4t) \quad \mu = 0.3$$
$$m_2 = 30 \quad F_2 = 50 \cos(0.8t)$$

Figure 3 shows the time history of m_1. Notice that the discontinuities in acceleration occur when the velocity changes sign. The magnitude of the acceleration always decreases across a discontinuity. Also note that the magnitude of a discontinuity corresponds to the magnitude of $|F_f|$ at that point. At the velocity zero crossings close to $t = 2$ and $t = 6$, $|F_f|$ is near zero, and the corresponding discontinuities in acceleration are small.

Friction also affects the overall magnitude of the acceleration curve. When the velocity and acceleration are of the same sign, friction acts against the applied force, and the magnitude of the acceleration is smaller with friction than without it. When the velocity and acceleration are of opposite sign, friction acts in the same direction as the applied force, and the acceleration with friction is of greater magnitude.

3.1.1. Numerical Integration of Discontinuous O.D.E.s

When integrating discontinuous ordinary differential equations, care must be taken to use the correct value of the derivative on each side of a discontinuity. Unfortunately, discontinuities generally occur inside an integration subinterval. A standard technique is to employ switching functions that flag the presence of a discontinuity in the last

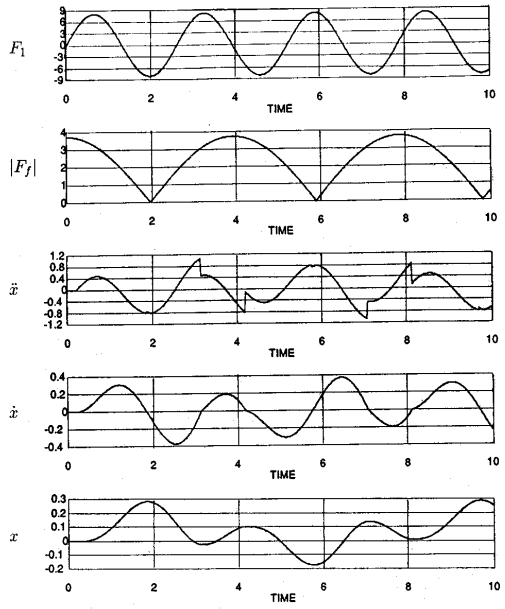

Fig. 3. Simulated time history of mass 1 with friction. Position is measured relative to a local frame centered in mass 2.

subinterval. For the initial value problem,

$$\dot{x} = f(x,t),$$
$$x(0) = x_0,$$

a *switching function*, $\phi(x,t)$, is defined such that $\phi(x,t) = 0$ when $f(x,t)$ is discontinuous and $\phi(x_n,t_n) \cdot \phi(x_{n+1},t_{n+1}) < 0$ implies a discontinuity in the subinterval $x_n \leq x \leq x_{n+1}$ (Fatunla 1988). For a velocity zero crossing, $\text{sgn}(\dot{q})$ is such a function.

In addition to detecting a discontinuity, the integrator must also provide a mechanism for locating the point of discontinuity within the subinterval. Integration up to the point of discontinuity is then repeated. The integration routine is then restarted from the discontinuity using the appropriate derivative value. Initially, small steps should be taken to accurately capture any transients that follow the discontinuity. If the friction model includes stiction (static friction), the integrator must also include tests to detect when sticking occurs. This is discussed in Sections 4.2 and 4.3.

Variable-step-size, variable-order methods are appropriate for integrating discontinuous equations. The plots appearing in Figure 3 were obtained using a method of this type. For synchronization purposes in real-time simulation and control, however, Morgowicz (1988) suggests the use of fixed-step-size methods. By choosing the controller period as a multiple of the fixed step size, the simulated robot state is available at controller sampling times.

To locate discontinuities occurring during the previous subinterval, Morgowicz uses linear interpolation. Approximate values of the state derivatives on both sides of the discontinuity are computed. They are used to reintegrate the subinterval in one step. Unless very fine motions are under consideration, simplifications of this type can give quite adequate simulation results. The time saved in simulating a given trajectory will depend on the number of velocity zero crossings involved.

3.2. *Implicitness of the Forward Solution*

In general, the inclusion of load-dependent Coulomb or static friction in the robot dynamic equations renders them implicit in the joint accelerations. The forward solution requires an iterative root-finding procedure (such as a modified Newton method) at each step of the integration to compute the accelerations. A hybrid-computer alternative to iteration is described in Gogoussis and Donath (1990b).

The cause of the implicitness is the dependence of friction on the magnitude of the normal force. The normal force itself is a function of the resultant force and moment at the joint. Expressed in a local coordinate frame, the components of the resultant force and moment can be formulated in terms of the joint positions, velocities, and accelerations. Just as with the net input forces or torques ($\tau - f$ in (3)), these components will be affine transformations of the accelerations.

If the direction of the normal force happens to be constant in the local frame, the normal force can be expressed as a function in which the net force and moment components appear linearly. This is true for friction in translational joints such as the X-Y positioning system described in the previous section and for axially loaded bearings when the axial load can be considered independently of radial load. Because the sign of the normal force can change, its absolute value must be used to obtain its magnitude.

When the direction of the normal force is not constant in a local joint coordinate frame, the magnitude of the normal force will involve the square root of sums of squares of net force and moment components. As an example, consider a radially loaded joint bearing. The load can take on any direction between zero and 2π radians. In the planar case, for a local frame attached to the bearing with z as the bearing axis, the magnitude of the normal force is

$$F_{\text{normal}} = \sqrt{F_x^2 + F_y^2}, \tag{7}$$

where F_x and F_y are the x and y components of the bearing reaction force. In three dimensions, there are multiple bearings at a joint, and one must consider joint geometry and reaction torques as well as reaction forces (Gogoussis and Donath 1988).

We see from the preceding paragraphs that Coulomb friction involves the absolute value or square root of sums of squares of acceleration-dependent terms. Substituting either type of expression into the original dynamic equation destroys its affine properties, rendering it implicit in the accelerations. Consequently, it is necessary to iteratively solve for joint accelerations at each time step of a simulation.

For this reason, simulation of load-dependent friction terms appears to be very time consuming. This is not necessarily the case. For small friction coefficients, the zero-friction accelerations can be used to start the iterative process. Even better, Morgowicz (1988) claims convergence in two iterations using as initial values the normal force magnitudes from the preceding time step. The cost of implicitness is significant, however. Using two iterations effectively requires two forward solutions in addition to solving the inverse problem once for those force and torque components needed to compute the normal forces.

3.2.1. *Implicitness Resulting From Absolute Value*

For those cases in which the magnitude involves only an absolute value, it is sometimes possible to avoid an iterative solution. This is an important case, because it applies to transmission elements that, when present, often dominate machine friction. The various cases are discussed below.

In the most restrictive case, if it can be shown that the sign of the normal force does not change for all allowed trajectories of the mechanism, the absolute value can be dropped. This is the case for the screw transmissions of the robot discussed in Section 4.3. The combination of gravity preloading and trajectory constraints ensures normal forces of constant sign.

A less restrictive case corresponds to the normal force being continuous when passing through zero. If the initial sign of the normal force is known (for instance, starting from rest, $\dot{q} = 0$), the absolute value can be dropped and a switching function that depends on the sign of the normal force, F_N, can be adjoined to the original equations. The function, $\mathrm{sgn}(F_N)$, can be used as the switching function. The resulting equations are explicit.

This is not the most general case, as normal forces can depend on the discontinuous joint accelerations. To prove the continuity of a normal force at its zero crossings, it would be sufficient to show that all friction-induced discontinuities in normal force preserve its sign. Although this may be true of many practical manipulators and trajectories, it may be difficult to prove. In addition, if the input torque, τ, is allowed to be discontinuous, it would also be necessary to show that the sign of the normal force is preserved for these discontinuities as well.

In the most general case, normal forces can change sign because of friction-induced discontinuities. A general solution technique follows. It can be adapted to handle input torque discontinuities as well.

As long as the joint velocities are of constant sign or remain zero, the normal forces are continuous functions, and their signs can be tracked with switching functions. Whenever a frictional discontinuity (i.e, a velocity zero crossing) occurs, the signs of the normal forces may change, and an implicit solution technique is in order. To investigate the solution of these equations, let us reformulate (3) using a Coulomb friction model:

$$\tau = D(q)\ddot{q} + h(q,\dot{q}) + f(q,\dot{q},\ddot{q}), \tag{8}$$

$$f(q,\dot{q},\ddot{q}) = M|A(q)\ddot{q} + b(q,\dot{q})|. \tag{9}$$

Here M is a diagonal matrix with diagonal elements $\mu_i \mathrm{sgn}(\dot{q}_i)$, and μ_i is the coefficient of friction associated with joint i. The system of equations can be more simply stated by replacing the unknown, $\ddot{q}$, by x:

$$Ax + \mathrm{Diag}[\mu_i]|Cx + d| = b, \tag{10}$$

in which A, C, b and d are known constants and $|\cdot|$ denotes vector absolute value, not norm. The solution set consists of all intersection points of the constraint equations.

For $\mu_i = 0$, the equations simplify to

$$Ax = b. \tag{11}$$

Each constraint equation describes a hyperplane in the space of joint accelerations, and there is always a unique solution, since A corresponds to the inertia matrix that is invertible.

For $\mu_i > 0$ and n joints, the constraints are V-shaped, $(n-1)$–dimensional half-hyperplanes. Their intersection may consist of multiple points in acceleration space. All solutions are consistent with the equations and represent the dissipation of energy by friction. The existence and uniqueness issues associated with Coulomb friction between rigid bodies have been studied in Lötstedt (1981), Rajan et al. (1987), Mason and Wang (1988), and Dupont (1992a,b). In the context of a single friction contact, these articles all demonstrate that for a sufficiently high friction coefficient, there may be no consistent solution or several. Dupont (1992a) shows that a single degree of freedom is sufficient to exhibit these problems and that the number of consistent solutions depends on the value of input force or torque. Mason and Wang (1988) address the case

of no consistent solution and model it as an impact with zero approach velocity. Dupont (1992b) addresses the case of multiple dynamic solutions and shows that for a system of finite stiffness, the extra dynamic solution is unstable. In summary, the existence and uniqueness problems associated with friction of the form of (9) are due to the rigid-body assumption.

For most cases of interest involving low-friction mechanisms, the Vs are nearly hyperplanar and their intersection consists of a single point. As suggested by Gogoussis and Donath (1990a), this solution can be found by a two-step iterative process. The signs of the terms in absolute values are hypothesized and a trial solution is obtained based on the hypothesis. The trial solution is then checked for consistency with the hypothesized signs of the absolute-value terms. In a maximum of 2^n iterations, the unique solution can be found. To minimize the number of iterations, the hypothesized signs can be taken as those of the previous time step or as those of the frictionless solution.

In summary, if $\text{sgn}(A(q)\ddot{q} + b(q, \dot{q}))$, the vector of normal force signs, is known, the equations can be solved explicitly using switching functions. When a velocity zero crossing occurs, (i.e., $\dot{q} \neq 0 \rightarrow \dot{q} = 0$ or $\dot{q} = 0 \rightarrow \dot{q} \neq 0$), the two-step iterative process can be used. This involves repeatedly hypothesizing the vector $\text{sgn}(A(q)\ddot{q} + b(q, \dot{q}))$ and solving for $\ddot{q}$ until a consistent solution is found. This technique is used in the discussion of transmission friction that follows.

4. Friction in Transmission Elements

Transmission components such as gears, screws, and harmonic drives are often used to convert high-speed, low-torque motor output to low-speed, high-torque joint motion. In these devices, not only is the direction of the frictional normal force fixed in the local coordinate frame, but also the force can be represented by a function in which the input torque, output torque, and rotor-inertia torque appear linearly. These torques are all present in the frictionless dynamic equations. Thus, no additional force or moment components need be computed.

A direct relationship exists between the effective input torque and the output torque (or force) and can be represented as an efficiency. The expression for the efficiency can replace the friction torque in the dynamic equations. In the following sections, the nature of these equations is examined in the context of a screw drive.

4.1. Example 2. Screw Drives: The Scalar Case

Screws are used to convert angular motion into linear motion. Typically, the screw rotates with the motor. The load is attached to the nut, which translates as the screw rotates. The losses in a screw transmission are due to the sliding motion between the screw and nut threads. A force analysis of the screw and nut can be found in many mechanical design texts (Spotts 1985). Whereas the output is a force, F, an output torque, τ, can be computed as the product

$$\tau = l\, F, \tag{12}$$

where the screw lead, l, is defined here as the distance the nut advances as the screw rotates through one radian. The efficiency is the ratio of output to input torques and is a function of thread geometry and the coefficient of friction between the screw and nut.

Before discussing screws in the context of robot dynamics, consider the simple system in Figure 4 for raising and lowering a mass, m. Summing torques on the screw, we get

$$\tau_a = J_{zz}\ddot{q} + \tau_l + \tau_f. \tag{13}$$

The term, τ_a, is the applied motor torque. The terms on the right side of this equation correspond to the screw inertial torque, the load (output) torque, and the friction torque. The displacement of the screw is given by q. The screw lead, l, relates the linear displacement of the mass, y, with q. The load torque is comprised of inertial and gravity components and is given by

$$\tau_l = (ml\ddot{q} + mg)l. \tag{14}$$

The friction torque, τ_f, can be eliminated from the torque equation by introducing the efficiency, η.

$$\eta = \frac{\tau_l}{\tau_{\text{in}}}, \tag{15}$$

$$\tau_{\text{in}} = \tau_a - J_{zz}\ddot{q}. \tag{16}$$

There are two expressions of efficiency, η_1 and η_2, for the cases of driving and backdriving the screw. These correspond to friction acting against and with τ_{in}, respectively. In the constant velocity case, they also correspond to raising and lowering the load.

$$\eta = \begin{cases} \eta_1 < 1, & \text{sgn}(\tau_l) = \text{sgn}(\dot{y}), \quad \text{Driving} \\ \eta_2 > 1, & \text{sgn}(\tau_l) = -\text{sgn}(\dot{y}), \quad \text{Backdriving} \end{cases} \tag{17}$$

Using the screw efficiency, the torque equation reduces to

$$\eta(\tau_a - J_{zz}\ddot{q}) = \tau_l. \tag{18}$$

Selection of the appropriate value of η requires the signs of both the velocity and the load torque. The sign of the load torque corresponds to the sign of the normal force of friction. For this scalar equation, it can be shown that a sufficient condition for solution existence and uniqueness is that the screw be of the low-friction overhauling type (Dupont 1992a). In the context of Figure 4, a positive torque would have to be applied to an

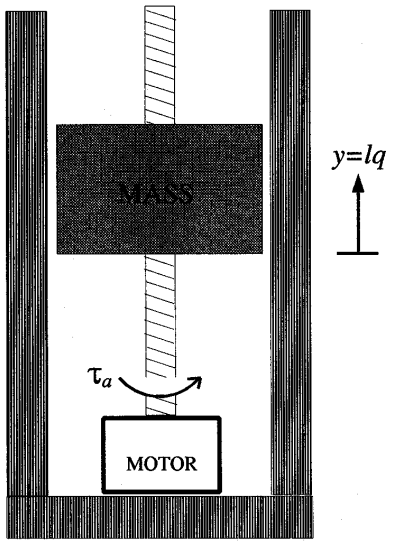

Fig. 4. Screw drive for positioning mass, m.

overhauling screw for the mass to descend with gravity at constant velocity.

The velocity and load torque must be included in the switching function used to integrate this equation. A velocity zero crossing would indicate the presence of a discontinuity in $\ddot{q}$ during the preceding integration subinterval. A load-torque zero crossing indicates a change in the slope of $\ddot{q}$ during the subinterval. Note that friction models expressing η as a function of such variables as position and velocity would not affect the solution procedure.

Notice how the screw inertial torque is not included as part of the load torque in (14). Motor rotor inertia should be treated in the same way. Because J_{zz} is typically small compared to the load torque, it is reasonable to question the importance of isolating it from the load torque. However, note that the screw lead, $l < 1$, amplifies the rotational screw inertia by the factor $1/l^2$.

The system in Figure 4 was simulated with the following parameter values chosen to clearly illustrate the dependence of acceleration on the signs of both velocity and load torque:

$$ml^2 = 50 \qquad \tau_{\text{in}} = 750\sin(4t)$$
$$J_{zz} = 5 \qquad g = 0$$
$$\eta_1 = .663 \qquad \eta_2 = 1.91$$

The simulation plots appear in Figure 5. The discontinuities in the acceleration, $\ddot{q}$, at velocity zero crossings are apparent. In addition, a change in the slope of $\ddot{q}$ occurs at load-torque zero crossings. Because gravity was taken to be zero, the load torque and the acceleration pass

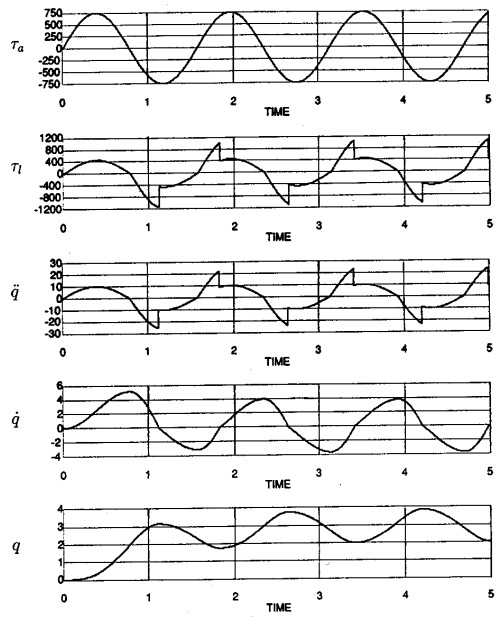

Fig. 5. Simulated time history of screw.

through zero simultaneously. One might suspect that if this were not the case, load-torque zero crossings would also cause discontinuities. However, examination of the equations shows that, irrespective of the value of g, zero crossings of τ_l cause discontinuities in jerk, $\dddot{q}$, but not in acceleration.

4.2. *Transmission Stiction*

Up to this point, friction at zero velocity has been neglected. Equation (18) is really only valid for nonzero velocities. A simple static friction model will be used to outline the forward dynamic solution of sticking joints.

At zero velocity, the static friction force assumes the magnitude and direction necessary to prevent motion. Its maximum magnitude is, in most cases, greater than or equal to the Coulomb value. Static values of the efficiencies can be computed using static friction coefficients.

$$\begin{aligned} \eta_{1s} &\leq \eta_1 < 1, \\ \eta_{2s} &\geq \eta_2 > 1. \end{aligned} \tag{19}$$

Consider when the screw is stuck because of friction. Both $\dot{q}$ and $\ddot{q}$ are zero. For the given value of load torque ($\tau_l = mgl$), there exists a band of applied torques for which no motion will ensue. This dead band is defined by

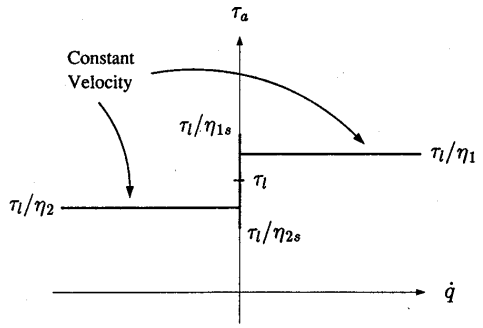

Fig. 6. Applied torque versus screw velocity showing stiction dead band for $\tau_\ell > 0$.

the inequalities

$$\begin{aligned} \tau_l/\eta_{2s} \;\le\; \tau_a \;\le\; \tau_l/\eta_{1s}, \qquad & \tau_l > 0 \\ \tau_l/\eta_{1s} \;\le\; \tau_a \;\le\; \tau_l/\eta_{2s}, \qquad & \tau_l < 0 \end{aligned} \tag{20}$$

and is pictured on the ordinate axis in Figure 6 for $\tau_l > 0$. Escape from static friction will occur when τ_a moves outside of this dead band. The direction of motion is determined by which inequality is violated. The screws used in robotic applications are overhauling in both the dynamic and static cases. This means that if the applied torque in Figure 4 is zero, the mass will descend under the force of gravity even if starting from rest.

So far, we have described the case when the screw is initially at rest. There is actually a second case when static friction must be considered. This occurs when the velocity is initially nonzero and changes sign during an integration subinterval. There are two possible discontinuities in acceleration at the zero crossing. In one, stiction occurs, forcing $\dot{q}$ and $\ddot{q}$ to zero. In the other, no stiction occurs, but the velocity changes sign. To determine which discontinuity occurs, the stiction inequality is evaluated at the time of the velocity zero crossing with $\ddot{q}$ assumed to be zero. If the applied torque at that instant falls outside the stiction dead band, then the value of η changes, but stiction does not occur.

In actuality, the friction model used in the preceding simulation included static friction. Stiction did not occur for two reasons. With $g = 0$, τ_l is zero at $t = 0$, and so no friction force can be generated. Second, the magnitude and frequency of τ_a are high enough that it is always outside the stiction dead band at velocity zero crossings.

4.3. Example 3. Screw Drives: The Vector Case

One example of a robot that uses screw drives is the Field Materiel Handling Robot (FMR) pictured in Figure 7. Constructed by Martin Marietta Aero and Naval Systems for the U.S. Army, the FMR is designed for palletized supply handling. This hydraulically driven, six-degree-of-freedom robot possesses a 25-foot reach and two-ton payload capacity. Because of stringent cycle time and transportability requirements, friction represented a potential challenge to the controller.

Roller screws are used to actuate the shoulder and elbow joints through closed kinematic chains, as depicted in Figure 8. Along with the hydraulic components, the screws are the dominant frictional elements. Roller screws differ from ordinary screws in that they include planetary, threaded rollers between the screw and the nut. The rollers substitute rolling and spinning friction for the much larger sliding friction that occurs between a simple screw and nut. Friction remains significant, however.

Although not addressed in the literature, theoretical friction models have been developed by roller screw manufacturers. These models are complex, highly application dependent, and proprietary (Lemor 1989). In their place, the manufacturer provides theoretical parameter values for the friction angle factor, K, the nominal diameter, d, and the screw lead, l, to be used in the efficiency equations for ordinary power screws, which are given below:

$$\eta_1 = \left(1 + \tfrac{Kd}{l}\right)^{-1} \qquad \eta_2 = \left(1 - \tfrac{Kd}{l}\right)^{-1}. \tag{21}$$

Consider first the case when the screw at joint i is moving:

$$\eta(\tau_i - \tau_i^s) = \sum_{j=1}^{n} d_{ij}\ddot{q}_j + h_i - \tau_i^s. \tag{22}$$

In this equation, τ_i^s represents the screw, and possibly motor rotor, inertial torque as seen by the motor. Because it is assumed that D and h include the screw inertia, it is explicitly subtracted from the right side of the equation.

By examining the Newton-Euler recursive equations, the screw inertial torque about the screw axis, τ^s, is found to be

$$\tau^s = e_3 \cdot \left(I_s\dot{\omega}_s + \omega_s \times (I_s\omega_s)\right). \tag{23}$$

Here, e_3 is a unit vector in the z-direction, I_s is the inertia tensor of the screw, and ω_s is the screw's angular velocity. All are expressed in a local coordinate frame attached to the screw. Furthermore, the cross-product term does not contribute, since, for the screw, $I_{xx} = I_{yy}$. The vector $\dot{\omega}_s$ is a function of the velocities and accelerations of the screw joint and all preceding joints. The general form of τ^s for a screw at joint i is

$$\tau_i^s = \left[a_{i1}(q),\ \ldots,\ a_{ii}(q),\ 0,\ \ldots,\ 0\right]\ddot{q} + b_i(q, \dot{q}). \tag{24}$$

The standard, open-chain Newton-Euler equations can be adapted for use in the forward and inverse dynamics of closed kinematic chains using a method such as that

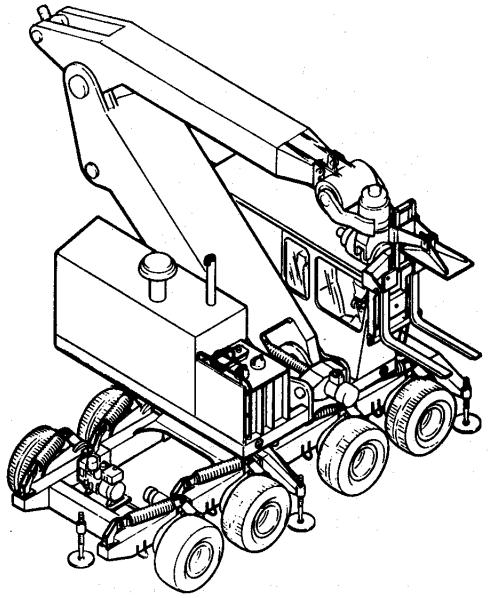

Fig. 7. The Field Materiel Handling robot (FMR).

described in Murray and Lovell (1989). The closed chains affect the term values, but not the form, of the preceding equation and those that follow.

Applying (22) and (24) to the system of equations yields

$$\begin{bmatrix} d_{1,1} & \cdots & \cdots & \cdots & \cdots & d_{1,n} \\ \vdots & & & & & \vdots \\ d_{i-1,1} & \cdots & \cdots & \cdots & \cdots & d_{i-1,n} \\ d_{i,1}+(\eta-1)a_{i1} & \cdots & d_{i,i}+(\eta-1)a_{ii} & d_{i,i+1} & \cdots & d_{i,n} \\ d_{i+1,1} & \cdots & \cdots & \cdots & \cdots & d_{i+1,n} \\ \vdots & & & & & \vdots \\ d_{n,1} & \cdots & \cdots & \cdots & \cdots & d_{n,n} \end{bmatrix} \times \ddot{q} + \begin{bmatrix} h_1 \\ \vdots \\ h_{i-1} \\ h_i+(\eta-1)b_i \\ h_{i+1} \\ \vdots \\ h_n \end{bmatrix} = \begin{bmatrix} \tau_1 \\ \vdots \\ \tau_{i-1} \\ \eta\tau_i \\ \tau_{i+1} \\ \vdots \\ \tau_n \end{bmatrix} \tag{25}$$

Thus, for a screw in motion, the form of the dynamic equations is reduced to that of the frictionless case.

Now we will consider the static case. Recall that when a screw is sticking, $\dot{q}_{\text{screw}} = \ddot{q}_{\text{screw}} = 0$. To determine if breakaway occurs, the same inequalities as the scalar case are employed. For screw i, the stiction dead band is given by

$$\begin{aligned} \tau_i^l/\eta_{2s} \le \tau_i \le \tau_i^l/\eta_{1s}, \quad \tau_i^l > 0, \\ \tau_i^l/\eta_{1s} \le \tau_i \le \tau_i^l/\eta_{2s}, \quad \tau_i^l < 0. \end{aligned} \tag{26}$$

In this case the load torque on screw i is given by

$$\tau_i^l = \sum_{j=1}^{n} d_{ij}\ddot{q}_j + h_i - \tau_i^s. \tag{27}$$

The screw inertial torque in the equation above is not necessarily zero because of contributions from the motion of preceding links.

The accelerations of the other joints are needed to solve for τ_i^l. They can be computed using the explicit equation

$$\begin{bmatrix} d_{1,1} & \cdots & d_{1,i-1} & d_{1,i} & d_{1,i+1} & \cdots & d_{1,n} \\ \vdots & & \vdots & \vdots & \vdots & & \vdots \\ d_{i-1,1} & \cdots & d_{i-1,i-1} & d_{i-1,i} & d_{i-1,i+1} & \cdots & d_{i-1,n} \\ 0 & \cdots & 0 & 1 & 0 & \cdots & 0 \\ d_{i+1,1} & \cdots & d_{i+1,i-1} & d_{i+1,i} & d_{i+1,i+1} & \cdots & d_{i+1,n} \\ \vdots & & \vdots & \vdots & \vdots & & \vdots \\ d_{n,1} & \cdots & d_{n,i-1} & d_{n,i} & d_{n,i+1} & \cdots & d_{n,n} \end{bmatrix} \times \ddot{q} + \begin{bmatrix} h_1 \\ \vdots \\ h_{i-1} \\ 0 \\ h_{i+1} \\ \vdots \\ h_n \end{bmatrix} = \begin{bmatrix} \tau_1 \\ \vdots \\ \tau_{i-1} \\ 0 \\ \tau_{i+1} \\ \vdots \\ \tau_n \end{bmatrix} \tag{28}$$

To enforce $\ddot{q}_{\text{screw}} = 0$, the ith rows of τ, D, and h (associated with the sticking screw joint) are set to 0, except for the (i,i)th element of D, which is set to 1.

Through systematic application of the preceding equations, the friction in any number of screw joints can be included. To solve for the accelerations, each row of the dynamic equation corresponding to a screw joint is modified according to either (25) or (28). The load torque can then be computed for each screw joint using (27). These values can be used to test for breakaway of sticking joints. For the FMR, there is no ambiguity in selecting η_i for screws in motion, because the signs of τ_i^l are fixed. If they were not, the iterative procedure described in Section 3.2 could be employed. Similar equations can be derived for other transmission elements, as well as for other forward solution techniques. (See Gogoussis and Donath [1988] for a derivation of harmonic drive efficiency.)

5. Combining Friction Terms

When a joint exhibits friction in addition to transmission friction, the dynamic equations can take on one of two

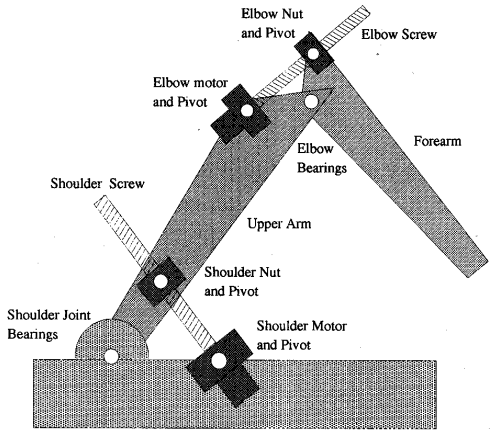

Fig. 8. Shoulder and elbow joints of the FMR. These joints are driven by roller screws through closed kinematic chains.

possible forms depending on the friction's source. Denoting the net motor torque by $\tau_m = \tau_i - \tau_i^s$, the load torque by τ_l, and the additional friction torque by τ_f, the two equations are

$$\tau_m = (1 \pm k)\tau_l + \tau_f, \tag{29}$$

$$\tau_m = (1 \pm k)(\tau_l + \tau_f/N). \tag{30}$$

The reciprocal of efficiency is represented by $(1 \pm k) > 0$. The signs apply to driving and backdriving the transmission, respectively. N is the effective transmission ratio of the joint. If, in (30), the friction coefficient is held constant instead of the friction torque and the friction torque is linearly related to $\dot{q}$ or $\ddot{q}$, then N should be squared. This would be true, for example, of viscous friction.

Equation (29) applies when the additional friction does not contribute to the load torque. For screws, this is true of any friction that must be overcome to spin the screw even when the nut is removed. In the FMR, this would be true of friction in the screw motors.

Equation (30) applies when the additional friction contributes to the transmission load torque. This would apply to friction in the bearings of the three pivot joints forming closed kinematic chains at the shoulder and elbow joints of the FMR (Fig. 8). While transmission friction amplifies and attenuates the additional friction term during driving and backdriving, respectively, division by the transmission ratio dominates.

Recognizing that τ_l is an affine transformation of $\ddot{q}$, we will solve for the discontinuity in τ_l, which will be linearly related to the discontinuity in acceleration. Making use of the following properties

$$\begin{aligned} &\text{Driving:} && \operatorname{sgn}(\tau_m) = \operatorname{sgn}(\tau_f) \\ &\text{Backdriving:} && \operatorname{sgn}(\tau_m) = -\operatorname{sgn}(\tau_f) \end{aligned}$$

we can compute $\triangle\tau_l$. For (29), the magnitude of the discontinuity in acceleration resulting from a velocity zero-crossing is linearly related to

$$\triangle\tau_l = \frac{2k\tau_m}{1-k^2} + \frac{2\tau_f}{1-k^2}. \tag{31}$$

Similarly for (30),

$$\triangle\tau_l = \frac{2k\tau_m}{1-k^2} + 2\tau_f/N \tag{32}$$

From (31), we can see that transmission friction increases the discontinuity in acceleration associated with τ_f (e.g., motor friction). From (32), it is clear that the transmission reduces the discontinuity associated with τ_f (e.g., bearing friction) by the factor N.

6. Experimental Friction Identification

By measuring the motor and load torques, we can solve for the total friction torque at a joint, which is given by

$$\tau_f = \tau_m - \tau_l.$$

In addition to transmission friction, the total friction will most likely include components of the form of both (29) and (30). If, for example, the friction torque is composed of components resulting from the screws, bearings, and motor, it can be expressed as

$$\tau_f = \pm k\tau_l \pm (1 \pm k)\tau_{bf}/N \pm \tau_{mf}. \tag{33}$$

Unless special model structures can be assumed for the motor and bearing friction terms, it will not be possible to ascertain the individual contribution of each friction source.

6.1. *Testing of the FMR*

Two types of test were used to experimentally determine the friction parameters for the FMR. To compute the friction torque, the motor torque at a joint was determined by measuring the chamber pressures of the hydraulic motors. The load torque was estimated using measured position and velocity data along with the estimated frictionless rigid-body dynamic model. The parameters for the frictionless model (inertias and link lengths) were obtained through a combination of direct measurement and solid modeling.

The first type of test, the *constant-velocity test*, involved moving single joints at constant velocity with

the remaining joints locked. In general, a high-gain velocity feedback controller is needed for this test. When repeated at different velocities for a given configuration and payload, the data points yield plots of friction force or torque versus velocity, such as shown in Figure 1. The dependence of friction on load was ascertained by collecting data for various payloads and configurations. Data were collected for both positive and negative velocities to detect any directional asymmetries such as have been reported by others (Armstrong 1988; Canudas De Wit et al. 1991).

A second type of test, the *breakaway test*, was used to determine stiction levels in each joint. Starting from rest, the motor torque for a single joint was slowly increased until motion was detected. The torque was then slowly decreased until the joint stuck. The test was performed for both directions of motion. In addition to determining whether a higher stiction level of friction exists, this test may reveal multivalued friction behavior such as that described in Hess and Soom (1990).

6.2. *Experimental Results*

This discussion focuses on the screw-driven shoulder and elbow joints of the FMR. At the time of testing, only open-loop control of the joints was possible. The servovalves' steady-state flow–versus-load curves for low flows, loads, and fixed currents are fairly flat, however. Thus, constant-velocity tests can be closely approximated by applying a constant current to the servovalve.

Because of open-loop control and project constraints, constant-current tests were run for a small range of low velocities for each joint. These were repeated for several payloads. In addition, breakaway tests for each joint were performed at several positions and payloads.

Plots of actual data for a representative constant-current test of the shoulder appear in Figure 9. The applied current is plotted in Figure 9*A*. This test included joint displacement in both directions, as shown in Figure 9*B*. Because the shoulder link is actuated through a closed kinematic chain, joint velocity is related to motor velocity through a position-dependent transformation. The effect of this transformation can be seen by comparing Figures 9*C* and 9*D*, which depict the motor and joint velocities, respectively. The motor torque and the load torque, the latter obtained from the estimated frictionless model, are shown in Figure 9*E*. The difference between these curves is the estimated friction torque.

To investigate the dependence of friction on normal force, friction torque versus load torque is plotted in Figure 9*F*. Also appearing in the figure are two lines fit by least squares to the positive and negative velocity data. To exclude the friction transients, the positive-velocity line was fit to data for time $t \in (10, 40)$ seconds. The negative-velocity line was fit for $t \in (50, 80)$. The equations of these lines are

$$|\tau_f| = \begin{cases} 0.50|\tau_l| + 464, & \dot{q} > 0, \\ 0.33|\tau_l| + 1037, & \dot{q} < 0. \end{cases} \tag{34}$$

These lines and the data from which they were obtained appear in Figure 9*G*. As expected, a significant dependence on load torque exists because of the screw transmission. In addition, a substantial directional asymmetry is apparent. The only asymmetry predicted by (33) relates to bearing friction:

$$|\tau_f|_{\dot{q}>0} - |\tau_f|_{\dot{q}<0} = \frac{2k\tau_{bf}}{N}. \tag{35}$$

Although this term does predict greater friction for positive velocities, bearing friction is expected to be small and transmission ratios relatively high. (The effective transmission ratios for the three pairs of bearings in the closed kinematic chain comprising the shoulder joint are configuration dependent.) Thus, the source of this asymmetry remains unclear. It is possible that the asymmetry is due to an unknown systematic error that generates a constant offset in either the motor or load torque of Figure 9*E*.

If we make the assumption that the bearing friction term in (33) is negligible, the expression for aggregate friction reduces to

$$\tau_f = \pm k\tau_l \pm \tau_{mf}. \tag{36}$$

Because motor friction may include both load-dependent and constant components, we can interpret the slopes in (34) as a combination of motor and transmission load dependence. To account for this, we write

$$\tau_{mf} = k_{mf}\tau_l + \tau_{mf}^c, \tag{37}$$

and letting $k' = k + k_{mf}$,

$$\tau_f = \pm k'\tau_l \pm \tau_{mf}^c. \tag{38}$$

Expressing the values of k' as efficiencies

$$\begin{array}{llll} k' = 0.50, & \eta_1 = 0.67, & \eta_2 = 2.0, & \dot{q} > 0 \\ k' = 0.33, & \eta_1 = 0.75, & \eta_2 = 1.5, & \dot{q} < 0 \end{array} \tag{39}$$

The manufacturer's theoretical range for η_1 is 0.8 to 0.9 for the shoulder and elbow screws. This tends to confirm the presence of load-dependent friction in addition to that of the transmission.

The results of the breakaway tests were surprising. To the accuracy of the FMR's sensors, the static level of friction was the same as the kinetic level observed in the constant-current tests. According to the manufacturer, the static efficiency can be up to 25% lower than the

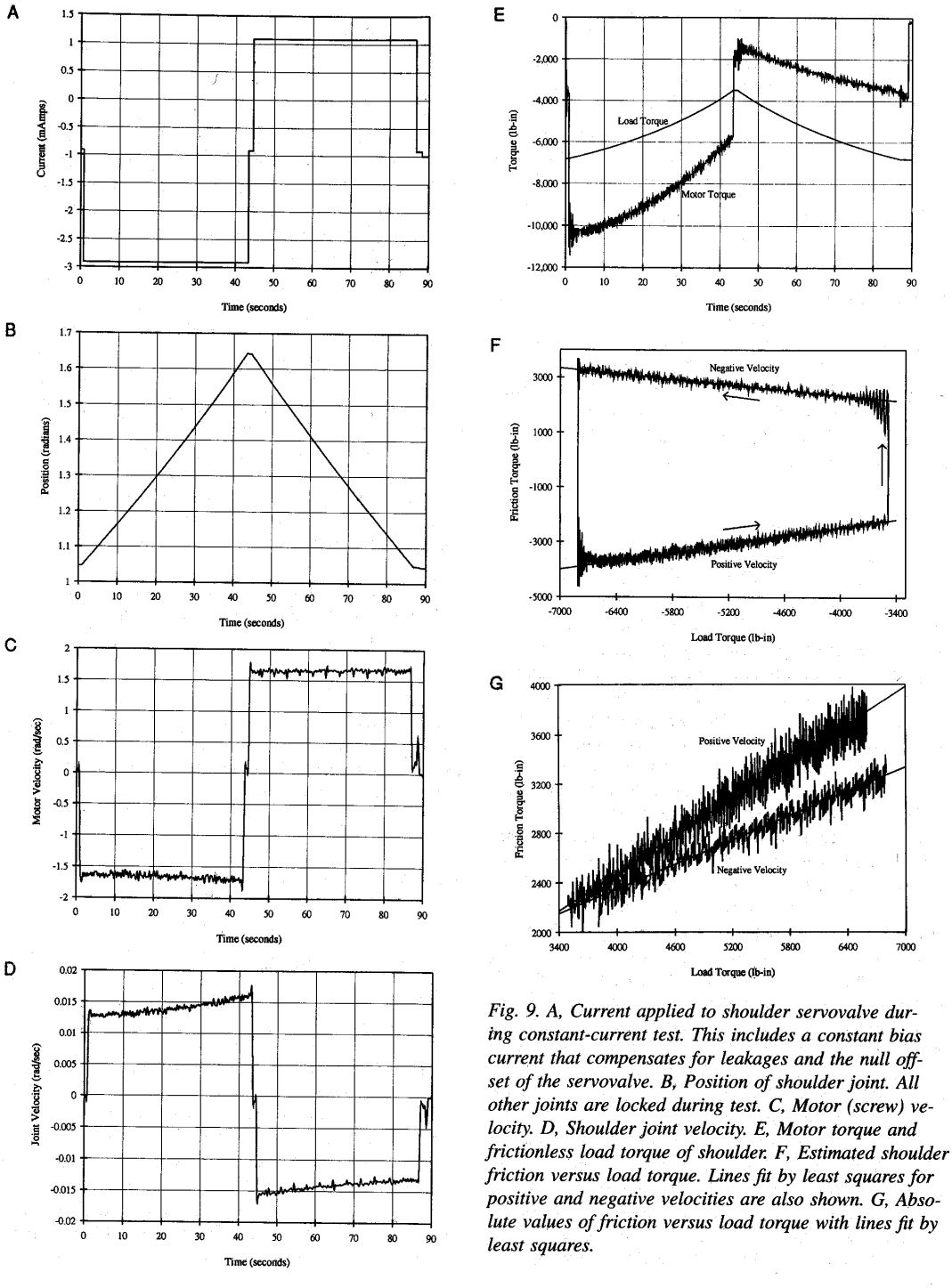

Fig. 9. A, Current applied to shoulder servovalve during constant-current test. This includes a constant bias current that compensates for leakages and the null offset of the servovalve. B, Position of shoulder joint. All other joints are locked during test. C, Motor (screw) velocity. D, Shoulder joint velocity. E, Motor torque and frictionless load torque of shoulder. F, Estimated shoulder friction versus load torque. Lines fit by least squares for positive and negative velocities are also shown. G, Absolute values of friction versus load torque with lines fit by least squares.

kinetic value (Lemor 1989). It is believed that the lack of a higher stiction level is due to a mechanical dither effect caused by the vibrations of the diesel engine and hydraulic pumps mounted on the FMR's truck body. In addition, the friction level at the onset of motion was the same as at motion cessation. Hence multivalued friction behavior was not observed.

6.3. *Load Dependence of Friction*

In contrast to other experimental work appearing in the robotics literature, friction was found to depend on load. In light of the load dependence of transmission models in general, this is not a surprising result. Two possible explanations are given here as to why load dependence was not observed by others. The arguments are based on transmission efficiency and preloading.

The relative motion between a power screw and its nut is that of pure sliding, which gives it perhaps the lowest efficiency of all transmission elements. Similar to screws, worm gear motion is predominantly sliding. In contrast, the relative motion between spur gears is predominantly rolling. As a result, the efficiency of spur gears is very high. Between these extremes are elements such as helical gears that combine rolling and sliding motion. The point of this comparison is that the load dependency of low-efficiency transmissions is easier to detect experimentally. Even though roller screws provide higher efficiencies than ordinary power screws, they are still relatively low-efficiency devices.

Methods of limiting or eliminating backlash are commonly used in robot transmissions. Preloading methods eliminate most backlash and also stiffen the transmission. Other methods, such as adjustable gear centers, eliminate only average backlash. In all cases, the goal is to simultaneously contact both sides of the screw threads or driving gear teeth. This is done at the expense of increased friction. For small applied loads, transmissions with backlash elimination, particularly preloading methods, can exhibit friction levels roughly independent of applied load. For example, roller screws can be preloaded by using two nuts that are separated by, and squeezed together against, a preload spacer. In the absence of an external load, each nut produces a friction torque proportional to the preload. As an external load is applied, the load on one nut increases by approximately half the external load, while the load on the other nut decreases by approximately half. Hence, for small external loads applied in either direction, the friction force is approximately constant. This is depicted in the load-deflection curves of Figure 10 (Lemor 1990). Similar behavior may occur with gear trains, although these are more complex to analyze because of their geometry.

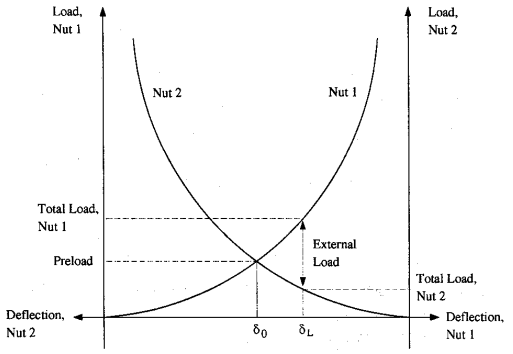

Fig. 10. Load versus deflection curves for the double nut of a preloaded roller screw.

In the FMR, preloading of the screws was unnecessary. The gravity load is sufficient to eliminate all backlash, given the maximum allowable acceleration of these joints. Without a preload, friction is directly proportional to applied load.

The disturbance-rejection capability of a hydraulic system for low flow rates and loads was manifested in the constant-current test data presented earlier. For moderate velocities and loads, simulation indicates that a nonlinear decoupling control law based on the rigid-body dynamics and a simplified hydraulic motor model is adequate to achieve critically damped response in the shoulder and elbow joints. To achieve appropriate response at high speeds and/or large loads, a feedforward, load-dependent friction term has been included in the FMR controller.

This example demonstrates that load-independent friction models can be inadequate. The load-dependent screw friction in the FMR can represent one third of the motor torque. Simulations indicate that the shoulder-screw load torque (and thus friction torque) can vary dynamically by $\pm 23\%$ from its average value during a typical unloaded trajectory. Of course, a comparison of loaded and unloaded trajectories would show an even greater variation in transmission friction. Simulations also show that the screw inertial torque at the elbow can be greater than 9% of τ_l during smooth trajectory segments and greater than 25% during transients.

7. Summary

In this article, the effect of friction on the solution of the forward dynamics problem is examined. Two factors are identified as making the problem more difficult than it is in the frictionless case. The differential equations can be discontinuous in the highest-order derivative terms (accelerations) and, for load-dependent friction, implicit in

the general case. Both concepts are clearly described and illustrated by examples.

In contrast to other work employing continuous approximations to discontinuous friction laws, a numerical integration scheme for discontinuous models that is based on switching functions is provided. In fact, this method is used in several commercial simulation packages.

In the case of load-dependent friction, the equations cannot always be solved explicitly for joint accelerations. In the general case, the accelerations must be obtained iteratively at each time step. While several researchers report convergence in two iterations, this more than doubles the number of operations at each time step.

When the direction of normal force is fixed in the local coordinate frame, the normal force appears as an absolute-valued expression. This is a very important case, as it includes transmission elements that can be dominant friction sources. This case is studied in detail, and the geometry of the solution set is described. It is shown that in certain situations the equations are explicit. For the general case, an iterative solution procedure that yields an exact solution in a finite number of iterations is described.

An efficiency formulation for transmission elements that has two benefits is introduced. First, friction can be included by simple modification of the frictionless solution procedure. Second, the computation of an inverse solution for normal force is avoided. These issues are described in the context of screw drives for which the forward dynamic equations with static and Coulomb friction are developed.

Experiments are described for measuring aggregate friction at a joint. A constant-velocity test is illustrated using experimental data from the FMR. This example shows a clear dependence of friction force on normal load.

With the price-to-performance ratio of digital computers dropping steadily, the choice of friction model can be based on actual friction behavior as opposed to ease of simulation. At the same time, the transmission example demonstrates that model accuracy is not always obtained at a great loss of efficiency. Friction models should be selected according to the behavior of the predominant friction sources in a particular robot. The necessary detail of the model for satisfactory results should be determined by the task and performance requirements.

Acknowledgments

This work was supported by the U.S. Army Research Office under grant DAAL03-89-K-0112 and by the IBM Corporation through a postdoctoral fellowship. I wish to thank Drs. Daniel W. Johnson and John J. Murray of Martin Marietta Aero and Naval Systems who provided valuable insights for this article and who, with their associates, performed the FMR experiments described here. My thanks to Pierre LeMor of SKF Component Systems for his discussions of roller screw behavior.

References

Adamson, A. W. 1982. *Physical Chemistry of Surfaces.* 4th ed. New York: John Wiley & Sons.

Armstrong, B. 1988. Friction: Experimental determination, modeling and compensation. *Proc. 1988 IEEE Int. Conf. on Robotics and Automation.* Philadelphia: IEEE, pp. 1422–1427.

Armstrong-Hélouvry, B. 1991. *Control of Machines with Friction.* Norwell, MA: Kluwer Academic Press.

Canudas De Wit, C., Noel, P., Aubin, B., Brogliato, B., and Drevet, P. 1991. Adaptive friction compensation in robot manipulators: Low velocities. *Int. J. Robotics Res.* 10(3):189–199.

Dahl, P. R. 1977. Measurement of solid friction parameters of ball bearings. *Proc. 6th Annual Symp. on Incremental Motion, Control Systems and Devices.* University of Illinois, pp. 49–60.

Dupont, P. 1991. Avoiding stick-slip in position and force control through feedback. *Proc. 1991 IEEE Int. Conf. on Robotics and Automation.* Sacramento: IEEE, pp. 1470–1475.

Dupont, P. 1992a. The effect of Coulomb friction on the existence and uniqueness of the forward dynamics problem. *Proc. 1992 IEEE Int. Conf. on Robotics and Automation.* Nice, France: IEEE, pp. 1442–1447.

Dupont, P. 1992b. The use of compliance to resolve the existence and uniqueness of the forward dynamics solution with Coulomb friction. *Proc. CSME Forum 1992.* Montreal, Canada: CSME, pp. 537–542.

Fatunla, S. O. 1988. *Numerical Methods for Initial Value Problems in Ordinary Differential Equations.* Boston: Academic Press.

Gogoussis, A., and Donath, M. 1987. Coulomb friction joint and drive effects in robot mechanisms. *Proc. 1987 IEEE Int. Conf. on Robotics and Automation.* Raleigh: IEEE, pp. 828–836.

Gogoussis, A., and Donath, M. 1988. Coulomb friction effects on the dynamics of bearings and transmissions in precision robot mechanisms. *Proc. 1988 IEEE Int. Conf. on Robotics and Automation.* Philadelphia: IEEE, pp. 1440–1446.

Gogoussis, A., and Donath, M. 1990a. A digital solution to the forward dynamics problem incorporating friction. Unpublished manuscript. Dept. of Mech. Engineering, University of Minnesota, Minneapolis.

Gogoussis, A., and Donath, M. 1990b. A method for the real time solution of the forward dynamics problem for

robots incorporating friction. *Trans. ASME, J. Dynam. Sys. Measurement Control* 112(4):630–639.

Haessig, D. A., and Friedland, B. 1990. On the modeling and simulation of friction. *Proc. 1990 American Control Conf.* San Diego: ASME, pp. 1256–1261.

Hess, D., and Soom, A. 1990. Friction at a lubricated line contact operating at oscillating sliding velocities. *ASME J. Tribology* 112:147–152.

Karnopp, D. 1985. Computer simulation of stick-slip friction in mechanical dynamic systems. *Trans. ASME J. Dynam. Sys. Measurement Control* 107(March):100–103.

Lemor, P. C. 1989. Personal communication, SKF Component Systems Corporation, Bethlehem, PA.

Lemor, P. C. 1990. Personal communication, SKF Component Systems Corporation, Bethlehem, PA.

Lötstedt, P. 1981. Coulomb friction in two-dimensional rigid body systems. *Zeitschrift für Angewandte Mathematik un Mechanik* 61:605–615.

Luh, J. Y. S., Walker, M. W., and Paul, R. P. C. 1980. On-line computational scheme for mechanical manipulators. *Trans. ASME J. Dynam. Sys. Measurement Control* 102(June):69–76.

Mason, M. T., and Wang, Y. 1988. On the inconsistency of rigid-body frictional planar mechanics. *Proc. 1988 IEEE Int. Conf. on Robotics and Automation.* Philadelphia: IEEE, pp. 524–528.

Morgowicz, B. 1988. Techniques for real-time simulation of robot manipulators. Ph.D. thesis, Univ. of Michigan, Dept. of Aerospace Engineering.

Murray, J. J., and Lovell, G. H. 1989. Dynamic modeling of closed-chain robotic manipulators and implications for trajectory control. *IEEE J. Robot. Automation* 5(4):522–528.

Rajan, V. T., Burridge, R., and Schwartz, J. T. 1987. Dynamics of a rigid body in frictional contact with rigid walls: Motion in two dimensions. *Proc. 1987 IEEE Int. Conf. on Robotics and Automation.* New York: IEEE, pp. 671–677.

Rice, J. 1983. *Numerical Methods, Software and Analysis—IMSL Reference Edition.* New York: McGraw-Hill.

Ruina, A. L. 1983. Slip instability and state variable friction laws. *J. Geophys. Res.* 88:10359–10370.

Spotts, M. F. 1985. *Design of Machine Elements.* 6th ed. Englewood Cliffs, NJ: Prentice Hall.

Szeri, A. Z. 1980. *TRIBOLOGY Friction, Lubrication and Wear.* New York: McGraw-Hill.

Threlfall, D. C. 1978. The inclusion of Coulomb friction in mechanisms programs with particular reference to DRAM. *Mechanism Machine Theory* 13(4):475–483.

Walker, M., and Orin, D. 1982. Efficient dynamic computer simulation of robotic mechanisms. *Trans. ASME J. Dynam. Sys. Measurement Control.* 104(3):205–211.

Walrath, C. D. 1984. Adaptive bearing friction compensation based on recent knowledge of dynamic friction. *Automatica* 20(6):717–727.